ACS APPLIED MATERIALS & INTERFACES

Research Article

www.acsami.org

Synthesis of Zeolitic Imidazolate Framework Core–Shell Nanosheets Using Zinc-Imidazole Pseudopolymorphs

Wan-Chi Lee, Heng-Ta Chien, Yang Lo, Hao-Che Chiu, Tung-ping Wang, and Dun-Yen Kang*

Department of Chemical Engineering, National Taiwan University No. 1, Sec. 4, Roosevelt Road, Taipei 10617, Taiwan

Supporting Information

ABSTRACT: Zeolitic imidazolate frameworks (ZIFs) are an emerging class of microporous materials that possess an organic flexible scaffold and zeolite-like topology. The catalytic and molecular-separation capabilities of these materials have attracted considerable attention; however, crystal-shape engineering in ZIF materials remains in its infancy. This is the first study to report an effective method for tailoring the near-spherical crystal morphology of ZIF-8 using its leaf-like pseudopolymorph, ZIF-L. A thin, uniform layer of ZIF-8 is formed on ZIF-L through heterogeneous surface growth to produce a ZIF-L@ZIF-8 core–shell nanocomposite. This results in ZIF-8 with a crystal morphology comprising two-dimensional nanoflakes. We characterized the resulting core–shell crystals using a number of solid-state techniques, including powder X-ray diffraction, scanning electron microscopy, thermogravimetric analysis, and nitrogen physisorption. Approximately 16 mass% of ZIF-8 in the core–shell composites heterogeneous surfacely grown on ZIF-L core crystals. We also investigated the effects of zinc salts, which were used as a source of zinc in the formation of the ZIF-L@ZIF-8 core–shell nanocomposites. Finally, we assessed the CO_2 adsorption properties of ZIF-8, ZIF-L, and ZIF-L@ZIF-8 core–shell crystals, the results of which were used to deduce the dynamic and equilibrium adsorption characteristics of various microporous ZIF crystals. The core–shell materials present hybridized CO_2 uptake and diffusivity of the parent crystals. The proposed method for the synthesis of core–shell nanocomposites using pseudopolymorphic crystals is applicable to other ZIF systems.

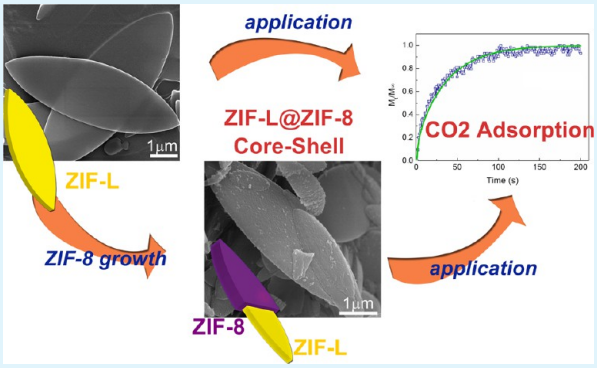

KEYWORDS: *zeolitic imidazolate framework, core–shell crystal, nanocomposite, pseudopolymorph, CO_2 adsorption*

INTRODUCTION

Zeolitic imidazolate frameworks (ZIFs) are a subfamily of metal–organic frameworks (MOFs), comprising imidazolate building units within a zeolite-type topology.[1,2] Since the discovery of the first MOF materials in 2003,[3] more than 150 ZIF structures have been identified.[4] The uniform microporosity, tunable surface functionality, and excellent thermal stability of ZIFs has led to their application in a variety of research areas, including molecular separation,[4−8] catalysis,[9−12] and gas storage.[13−15] ZIFs and zeolites are both classified as microporous materials with a pore size smaller than 2 nm. All ZIF structures have a zeolite analogue and zeolites have been investigated for far longer than have ZIFs. As a result, the development of ZIFs tends to follow that of zeolites. For more than two decades, zeolites have been prepared in membraneous forms for processes involving continuous gas separation,[16−20] and a number of recent reports have discussed the fabrication of pure ZIF membranes for the same applications.[4,21−24] Nonetheless, there are many areas of research in which zeolites are well-developed and ZIFs remain in their infancy, such as the engineering of crystal shape and micromorphology. The engineering the crystal shape and micromorphology of zeolites is intended to enhance their performance for targeted applications. For example, zeolite crystals with mixed micro- and meso-porosity have been developed to facilitate mass transfer in heterogeneous catalysis.[25−28] Zeolite crystals with a more complex hierarchical microstructure have also been created.[20,29−32] Researchers have also reported the tuning of crystal aspect ratio to improve the molecular separation performance of zeolite-containing membranes.[33−38] Zeolite–zeolite core–shell nanocomposites have been used as a tool for engineering molecular diffusion properties.[39−42]

Despite the numerous methods that have been developed for engineering the crystal shape and morphology of zeolites, far less effort has been dedicated to achieving similar results in ZIFs. In the last five years, only a few studies have reported success in the creation of hierarchical microstructures in ZIFs.[43−45] Several zeolite–ZIF, polymer–ZIF, and ZIF–ZIF core–shell composites for catalysis and electrochemistry have been reported in recent years.[46−48] Methods for fine-tuning the crystal morphology by controlling the relative growth rate among multiple crystal facets has also been studied; however,

Received: May 14, 2015
Accepted: August 4, 2015
Published: August 4, 2015

DOI: 10.1021/acsami.5b04217
ACS Appl. Mater. Interfaces 2015, 7, 18353−18361

this had not yet produced a pronounced change in the shape of the crystals.[49−51] A generalized approach to the engineering of crystal shape in ZIF materials has yet to be developed.

Herein, we report a new approach to the engineering of ZIF crystal shape through the heterogeneous surface growth of ZIF-8 on ZIF-L nanosheets to create layered ZIF-L@ZIF-8 core−shell nanocomposites. The crystals of pure ZIF-8 are nearly spherical (3D), which enables the synthesis of a hybrid material of ZIF-L@ZIF-8 core−shell crystals possessing the functionality of ZIF-8 but in a layered (2D) crystal shape. ZIF-8 is among the most widely studied ZIF materials with a zeolite SOD topology. ZIF-L has recently been identified as a pseudopolymorph of ZIF-8.[52−54] ZIF-L and ZIF-8 are both composed of zinc and 2-methylimidazole (2-MIM) but differ with regard to Zn/2-MIM ratio and crystal morphology (spherical for ZIF-8 and leaf-like for ZIF-L).[52,53] Compared to ZIF-8, ZIF-L presents far lower porosity (in nitrogen physisorption at 77K) but similar CO_2 adsorption uptake at room temperature.[52,53] High CO_2-to-CH_4 adsorptive selectivity (>10)[52] also make ZIF-L a promising material for natural gas separations. This work was based on the hypothesis that pseudopolymorphism between ZIF-8 and ZIF-L could enhance heterogeneous surface crystal growth in ZIF-8 on ZIF-L for the creation of core(ZIF-L)-shell(ZIF-8) crystals. The synthesis of ZIF-L@ZIF-8 nanocomposites could also be considered an effective tool for shaping ZIF-8 crystals into a 2D nanoflake micromorphology. The ZIF-L@ZIF-8 nanocomposites were carefully characterized using a variety of solid-state techniques, including scanning electron microscopy, X-ray diffraction, nitrogen physisorption, and thermal gravimetric analysis. We investigated the effects of zinc salts on the heterogeneous surface growth of ZIF-8 over ZIF-L. Finally, the dynamics of CO_2 adsorption in pure ZIF-8 and ZIF-8 and ZIF-L@ZIF-8 crystals were evaluated with regard to their effectiveness in engineering the gas adsorption properties of ZIF materials.

EXPERIMENTAL SECTION

Synthesis of ZIF-L. Pure ZIF-L crystals were synthesized using a method outlined in a previous report,[52] with some modifications. Briefly, 1.30 g of 2-methylimidazole (2-MIM) was added to 40 mL of deionized water, and in a separate solution, 0.59 g of zinc nitrate ($Zn(NO_3)_2{\cdot}6H_2O$) was added to the same amount of deionized water. The two solutions were mixed by pouring the zinc nitrate solution into the 2-MIM at a Zn:2-MIM:water molar ratio =1:8:2241. The mixture was stirred at room temperature for 4 h and then subjected to centrifugation at 10000 rpm for 20 min. The supernatant was decanted and the precipitate washed using deionized water. This purification procedure was repeated three times. The final solid-state product was stored in an oven at 105 °C.

Synthesis of ZIF-8. ZIF-8 crystals of two sizes were synthesized. The method used for the synthesis of ZIF-8 with a crystal size in the tens of nanometers was adopted from a previous report[55] with minor modifications. Briefly, 0.66 g of 2-methylimidazole (2-MIM) was added to 11 g of methanol, and in a separate solution, 0.3 g of zinc nitrate ($Zn(NO_3)_2{\cdot}6H_2O$) was added to the same amount of methanol. The two solutions were mixed by pouring the zinc nitrate solution into the 2-MIM with a Zn/2-MIM/methanol molar ratio = 1:8:681. The solution was then stirred at room temperature for 24 h and subjected to centrifugation at 10000 rpm for 20 min. The supernatant was decanted and the precipitate washed using methanol. This purification procedure was repeated three times. The final solid-state product was stored in an oven at 105 °C.

The method used in the synthesis of ZIF-8 with a crystal size of several micrometers was adopted from a previous report[56] with minor modifications. The control over the crystal size of ZIF-8 can be found in the previous reports.[57−60] Briefly, 7.7 g of 2-methylimidazole (2-MIM) was added to 40 mL of deionized water, and in a separate solution, 0.4 g of zinc nitrate ($Zn(NO_3)_2{\cdot}6H_2O$) was added to the same amount of deionized water. The two solutions were mixed by pouring the zinc nitrate solution into the 2-MIM at a molar ratio of Zn/2-MIM/water = 1:70:3305. This was then stirred at room temperature for 24 h before undergoing centrifugation at 10 000 rpm for 30 min. The supernatant was decanted and the precipitate washed using deionized water. This purification procedure was repeated three times. The final solid-state product was stored in an oven at 105 °C. In this study, micrometer-sized ZIF-8 crystals were used only for CO_2 adsorption measurements.

Synthesis of ZIF-L@ZIF-8 Core−Shell Nanocomposites. Briefly, 0.5 g of as-synthesized ZIF-L crystals were mixed with 0.3 g of zinc nitrate in 11 g of methanol. A separate solution was prepared by dissolving 0.66 g of 2-MIM in 11 g of methanol. The molar ratio of Zn/2-MIM/methanol in the liquid phase of the mixture was 1:8:681. The two solutions were then combined and the resulting mixture was held at room temperature for 24 h without agitation. The mixture was subjected to centrifugation at 10 000 rpm for 6 min, during which time most ZIF-L and the core−shell crystals were left in the precipitate and ZIF-8 crystals remained in the supernatant. The supernatant was decanted and the precipitate washed using methanol. This purification procedure was repeated three times. Five other zinc salts ($Zn(OAc)_2$, $Zn(acac)_2$, ZnCl, $ZnBr_2$, and $ZnSO_4$) were also used for the synthesis of core−shell composites. The Zn/2-MIM/methanol molar ratio in the synthesis solution and the synthesis procedure were the same as those used in the synthesis involving $Zn(NO_3)_2$. Unless elsewhere stated, the ZIF-L@ZIF-8 core−shell nanocomposites described in the manuscript refer to the product synthesized from $Zn(NO_3)_2$.

Characterization Methods. Powder X-ray diffraction (XRD) was performed using a Rigaku diffractometer with Cu Kα radiation operating at 50 mA and 60 kV with a scanning rate of 10° 2θ min^{-1}. The scanning range was from 5° to 40° 2θ with a step size of 0.02 °. The solid-state samples were imaged using a Hitachi S-4800 Field Emission scanning electron microscope (SEM). Thermogravimetric analysis (TGA) was performed using a PerkinElmer's Pyris 1 using approximately 5 mg of the samples under nitrogen diluted air. During testing, the temperature was elevated from room temperature to 800 °C at a ramp rate of 10 °C/min. Nitrogen physisorption isotherms were obtained using a Micromeritics ASAP 2010 analyzer at 77K. The samples were placed in an analysis tube and degassed under 20 Torr at 80 °C overnight prior to physisorption measurement. FT-IR spectra were recorded using a JASCO FT/IR-6700 spectrometer with a Ge coated KBr beam splitter. Each FT-IR spectrum was obtained from 100 scans at a resolution of 4 cm^{-1}. Measurements of CO_2 adsorption were conducted using a proprietary apparatus based on the piezometric method.[61,62] Samples was placed in an analysis chamber and degassed under vacuum (approximately 0.01 Torr) overnight prior to measurement, at which time approximately 5.6 Torr of CO_2 was introduced into chamber. The pressure in the analysis chamber was monitored for 1 h. The adsorption uptake of the sample as a function of time was then deduced according to the drop in pressure within the chamber according to the conservation of mass for CO_2.

RESULTS AND DISCUSSION

Crystal Morphology of ZIF-L@ZIF-8 Core−Shell Nanocomposites. Figure 1 presents SEM images of pure ZIF-8, pure ZIF-L, and ZIF-L@ZIF-8 core−shell crystals. Clearly, the crystals of ZIF-8 are nearly spherical in shape, whereas ZIF-L appears as leaf-like 2D crystals. Figures 1c and 1d suggest that the as-synthesized ZIF-L crystals are translucent with a glossy surface, which is likely due to a crystal structure that is more densely packed than that of the ZIF-8.[52,53] The pure ZIF-L crystals are approximately 5 μm in length and 300 nm in thickness. The ZIF-L@ZIF-8 core−shell nanocomposites present a crystal appearance distinct from as-synthesized ZIF-L with the surface of the core−shell crystals appearing rough and opaque. This may be an indication of the (anticipated) occurrence of

DOI: 10.1021/acsami.5b04217
ACS Appl. Mater. Interfaces 2015, 7, 18353−18361

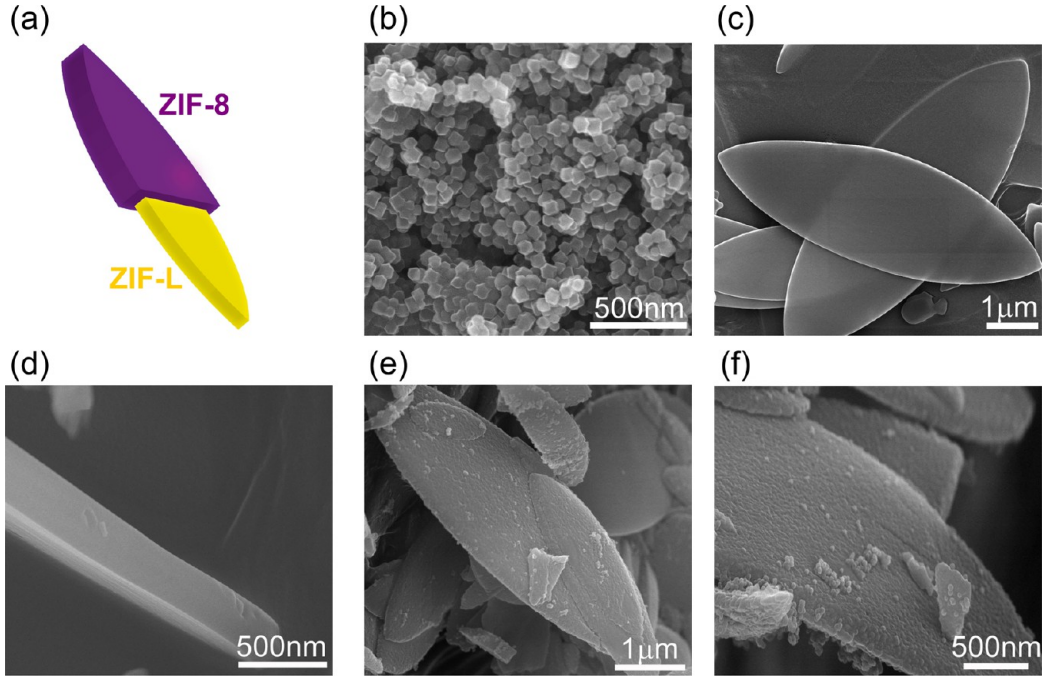

Figure 1. (a) Illustration of ZIF-L@ZIF-8 core−shell nanocomposites and SEM images of (b) as-synthesized ZIF-8, (c and d) as-synthesized ZIF-L, and (e and f) ZIF-L@ZIF-8 core−shell crystals.

heterogeneous surface growth of ZIF-8 on ZIF-L crystals as well the growth of ZIF-8 crystals from the surface of ZIF-L. The size of the crystal in ZIF-L and ZIF-L@ZIF-8 core−shell nanocomposites were nearly identical, which suggests that only a thin layer of ZIF-8 formed on ZIF-L. However, SEM images of ZIF-L@ZIF-8 core−shell nanocomposites in Figure 1e and 1f indicate the occurrence of a process other than heterogeneous surface growth. Specifically, these results suggest that ZIF-8 crystals growing freely in the solvent accumulated on the surface of the ZIF-L following the removal of the solvent. If this were the case, then the interaction between ZIF-8 and ZIF-L crystals would only be physical (not chemical), such that ZIF-L@ZIF-8 core−shell nanocomposites would fail to form.

To confirm the formation of core−shell crystals, we conducted a control experiment involving the physical mixing of as-synthesized ZIF-L and ZIF-8 (nanosized crystals) samples. Figure 2 presents SEM images of the control samples. Figure 2a illustrates the physical mixture of ZIF-L and ZIF-8, involving equal masses of ZIF-L and ZIF-8 in methanol without further purification. The smoothness of the ZIF-L crystal surface appears comparable to that of the as-synthesized ZIF-L (Figure 1c and 1d) and was distinct from ZIF-L@ZIF-8 core−shell nanocomposites (Figure 1e and 1f). In Figure 2a, the physical mixture of ZIF-8 and ZIF-L appeared as two types of distinct bulk crystals in contrast to what is shown in Figure 1e and 1f. This is a possible indication that the nanocomposites in Figure 1e and 1f were actually formed via the heterogeneous surface growth of ZIF-8 on ZIF-L. Figure 2b presents an SEM image of the supernatant obtained from the physical mixture of as-synthesized ZIF-8 and ZIF-L under centrifugation (10000 rpm for 6 min) to isolate the ZIF-8 crystals. The precipitate of this physical mixture after centrifugation revealed ZIF-L as the major species (Figure 2c and 2d). The ZIF-L crystals in Figure 2c appear as glossy as those in Figure 1c and 1d, which suggests that the physical mixing of ZIF-8 and ZIF-L is unlikely to alter the appearance of the ZIF-L crystals. This series of experiments demonstrates the effectiveness of using centrifugation for the separation of ZIF-L (precipitate) and ZIF-8 (supernatant) crystals. The SEM images in Figure 1e and 1f were collected from the precipitate after centrifugation, which rules out the possibility that the crystals were the result of ZIF-8 physically settling on the ZIF-L crystals. This provides evidence to support the supposition that the crystals in Figure 1e and 1f are indeed ZIF-L@ZIF-8 core−shell nanocomposites. Additional SEM images of ZIF-L and ZIF-L@ZIF-8 core−shell nanocomposites are presented in the Supporting Information (Figure S1).

Crystallinity, Porosity, Thermal Stability of ZIF-L@-ZIF-8 Core−Shell Nanocomposites. The crystallinity of as-synthesized ZIF-8, ZIF-L, and ZIF-L@ZIF-8 core−shell nanocomposites was evaluated by powder X-ray diffraction (XRD), as shown in Figure 3. The diffraction patterns obtained from ZIF-8 and ZIF-L samples are in agreement with previous findings in the literature.[52,53] As expected, the ZIF-L@ZIF-8 core−shell nanocomposites present XRD patterns representing a combination of signals from pure ZIF-8 and ZIF-L. This suggests that the synthesis of the core−shell preserved the crystallinity of ZIF-L as a core material. XRD analysis provides a qualitative measure of the existence of ZIF-8 and ZIF-L in the core−shell composites, whereas nitrogen physisorption provides quantitative analysis related to the relative quantities of ZIF-8 and ZIF-L in the nanocomposites. Figure 4 presents nitrogen physisorption isotherms of pure ZIF-8, ZIF-L, and ZIF-L@ZIF-8 core−shell crystals, indicating a microporose structure on the pure ZIF-8 possess and almost no pores on pure ZIF-L. These findings are in agreement with those reported in previous studies.[53] The porosity of ZIF-L@ZIF-8 core−shell composites lies between that of the as-made ZIF-8 and ZIF-L crystals but much closer to ZIF-L. The mass fraction of the ZIF-8 in the ZIF-L@ZIF-8 core−shell crystals was determined to be 16 mass% by deriving the micropore volume from the physisorption results. This is consistent with the results suggested by the SEM images (Figure 1), in which

DOI: 10.1021/acsami.5b04217
ACS Appl. Mater. Interfaces 2015, 7, 18353−18361

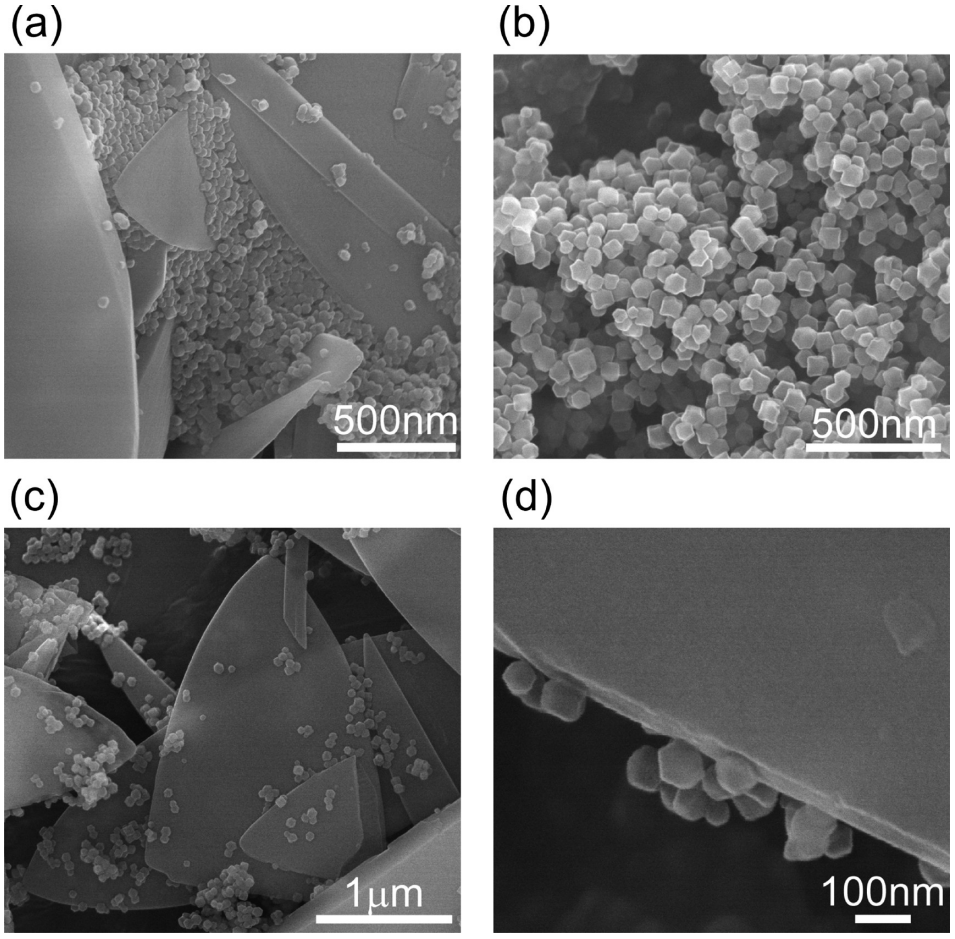

Figure 2. SEM images of (a) unseparated physical mixture of ZIF-L and ZIF-8, (b) supernatant, and (c and d) precipitate of physically mixed ZIF-L and ZIF-8 solution following centrifugation at 10 000 rpm for 6 min.

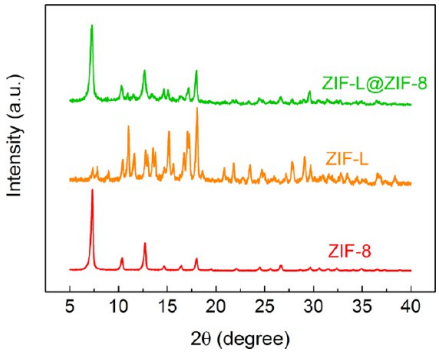

Figure 3. XRD patterns of ZIF-8, ZIF-L, and ZIF-L@ZIF-8.

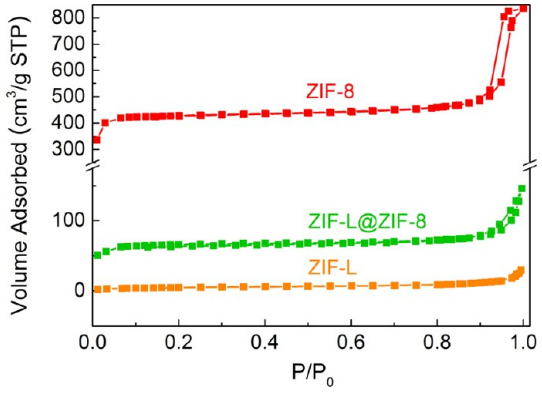

Figure 4. Nitrogen physisorption isotherms of ZIF-8, ZIF-L, and ZIF-L@ZIF-8.

only a skin layer of ZIF-8 formed on the exterior of ZIF-L. Thermogravimetric analysis (TGA) can also be used to obtain a semiquantitative measure of the relative quantities of ZIF-L and ZIF-8 crystals in the core−shell composites. The curves of mass loss and heat flux as a function of time (as deduced from TGA) are presented in the Supporting Information (Figure S2 and S3). The mass loss and heat flux curves from ZIF-L@ZIF-8 core−shell nanocomposites resemble those obtained from ZIF-L crystals, which suggests that ZIF-L is the major component in the composites. This observation is in good agreement with the characterization results deduced from nitrogen physisorption. The FT-IR spectra of ZIF-8, ZIF-L, and ZIF-L@ZIF-8 core−shell crystals are summarized in the Supporting Information (Figure S4). The three FT-IR spectra are highly similar, because the functional groups presented in these crystals are nearly identical. However, the ZIF-8 crystals show more pronounced aromatic and aliphatic C−H stretching in comparison to ZIF-L and ZIF-L@ZIF-8 crystals.

Effects of Zinc Salts on the Formation of ZIF-L@ZIF-8 Core−Shell Nanocomposites. The ZIF-8 shell in the ZIF-L@ZIF-8 core−shell nanocomposite was grown using zinc nitrate as the source of zinc. In this section, we discuss the

DOI: 10.1021/acsami.5b04217
ACS Appl. Mater. Interfaces 2015, 7, 18353−18361

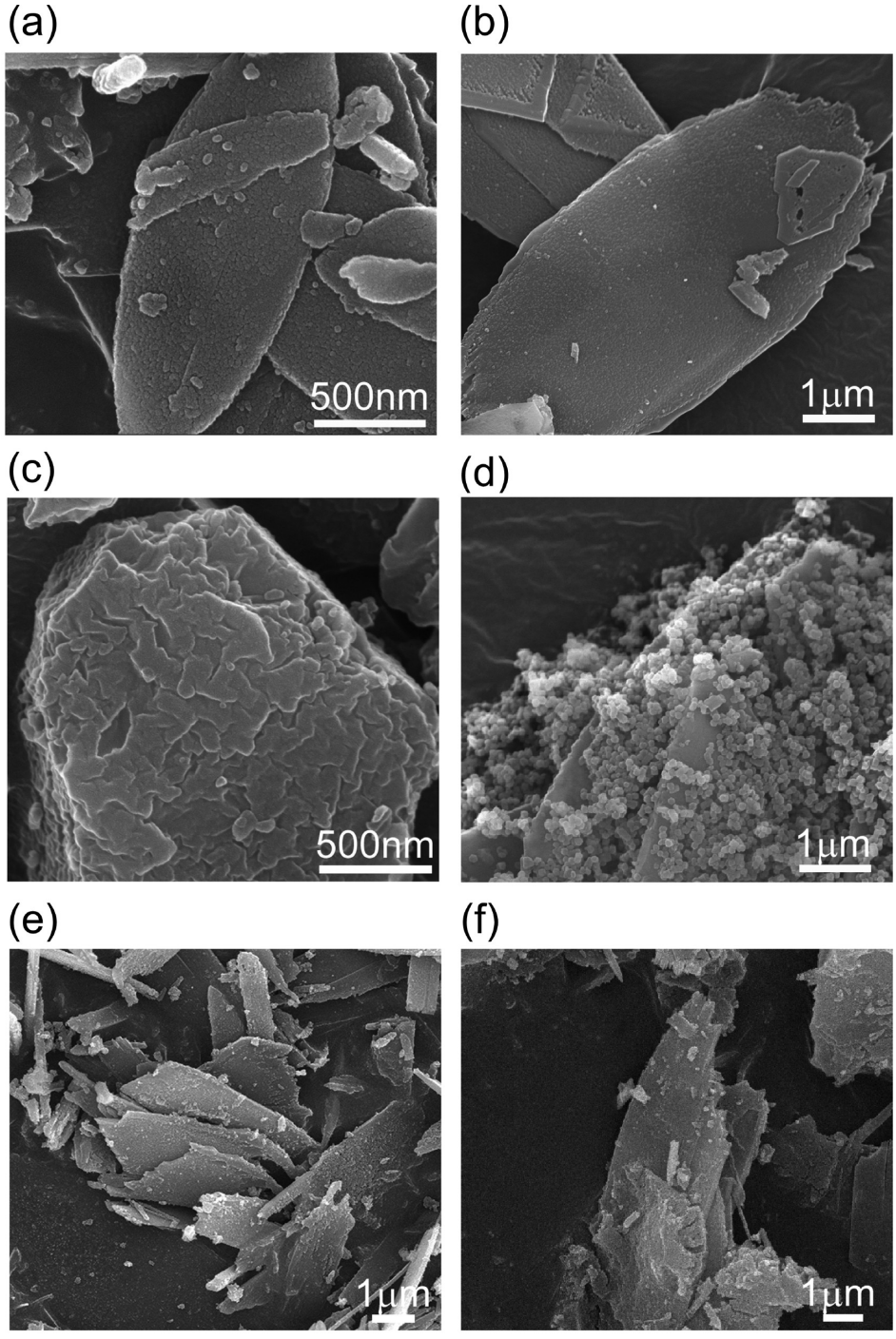

Figure 5. SEM images of ZIF-L@ZIF-8 core−shell crystals synthesized from (a) $Zn(NO_3)_2$, (b) $Zn(OAc)_2$, (c) $Zn(acac)_2$, (d) ZnCl, (e) $ZnSO_4$, and (f) $ZnBr_2$.

heterogeneous surface growth of ZIF-8 on ZIF-8 using the following zinc salts: $Zn(NO_3)_2$, $Zn(OAc)_2$, $Zn(acac)_2$, ZnCl, $ZnSO_4$, and $ZnBr_2$ for the synthesis of core−shell nanocomposites. SEM images of the six resulting products are presented in Figure 5. The use of zinc nitrate or zinc acetate resulted in nanocomposites with a well-defined ZIF-L leaf-like shape. In contrast, the use of zinc acetylacetonate, zinc chloride, zinc sulfate, and zinc brimode resulted in nanocomposites with a poorly defined microstructure. Powder X-ray diffraction was used to gain insight into the microstructure of these six products (Figure 6). XRD patterns of the products synthesized using $Zn(NO_3)_2$ or $Zn(OAc)_2$ revealed a combination of ZIF-L and ZIF-8 patterns, which suggests the coexistence of these two crystals in the product. This may imply that the use of these two zinc salts resulted in the successful formation of ZIF-L@ZIF-8 core−shell nanocomposites. In contrast, the XRD patterns of the product made using $Zn(acac)_2$, ZnCl, $ZnSO_4$, and $ZnBr_2$ revealed only ZIF-8 signals. This suggests that these salts caused the decomposition of ZIF-L during the synthesis process, thereby leaving only ZIF-8.

CO_2 Adsorption. Pure ZIF-8 (micrometer-sized crystals), pure ZIF-L, and ZIF-L@ZIF-8 core−shell crystals were

DOI: 10.1021/acsami.5b04217
ACS Appl. Mater. Interfaces 2015, 7, 18353−18361

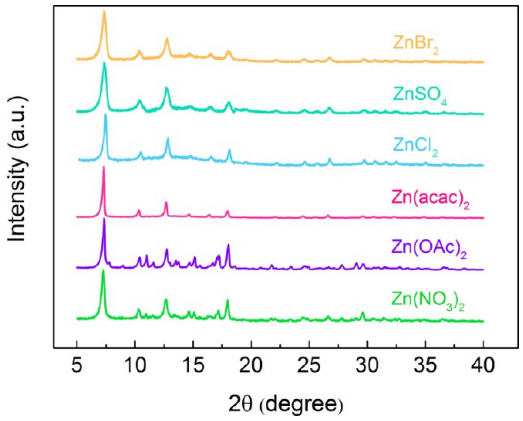

Figure 6. XRD patterns of ZIF-L@ZIF-8 core−shell crystals synthesized from various zinc salts.

subjected to CO_2 adsorption experiments. To deduce the intrinsic molecular diffusivity of CO_2 in these three crystals, we performed adsorption experiments under the rather low pressure of 5.6 Torr and recorded the dynamics of the adsorption (Figure 7). Typically, smaller crystals resulted in a shorter time scale for the adsorption process. To ensure that the adsorption dynamics were detectable by the instrument, we employed micrometer-sized ZIF-8 crystals, as opposed to nanosized ones. SEM images of the micrometer-sized ZIF-8 crystals are presented in the Supporting Information (Figure S5). Figure 7 illustrates the similarities in the time scales associated with CO_2 adsorption using ZIF-8, ZIF-L, and ZIF-L@ZIF-8 core−shell nanocomposites. Quantitative analysis of this effect was achieved by deducing the diffusivity of CO_2. We employed the following equation used to describe the transient adsorption uptake for spherical adsorbents in order to fit the adsorption dynamics in ZIF-8:[61]

$$\frac{M_t}{M_\infty} = 1 - \frac{6}{\pi^2}\sum_{n=0}^{\infty}\left(\frac{1}{n}\right)^2 \exp\left(-\frac{n^2\pi^2 Dt}{R^2}\right) \quad (1)$$

where M_t is the transient adsorption uptake, M_∞ is the equilibrium uptake, D is diffusivity, and R represents the crystal radius. In contrast, we employed the equation used to describe the adsorption dynamics in slab-shaped adsorbents to fit the adsorption dynamics in ZIF-L and ZIF-L@ZIF-8 core−shell nanocomposites:[61]

$$\frac{M_t}{M_\infty} = 1 - \frac{8}{\pi^2}\sum_{n=0}^{\infty}\left(\frac{1}{2n+1}\right)^2 \exp\left(-\frac{(2n+1)^2\pi^2 Dt}{4L^2}\right) \quad (2)$$

where L is the thickness of the slab-shaped crystal. When applying eqs 1 and 2, R = 750 nm was used to fit the adsorption dynamics using ZIF-8, whereas L = 150 nm was used to fit the adsorption dynamics using ZIF-L. These characteristic lengths were determined using the average particle sizes observed in the SEM images (Figure S5), in which both ZIF-8 and ZIF-L crystals show a narrow particle size distribution. The derived CO_2 diffusivity and equilibrium uptake values are summarized in Table 1.

According to the CO_2 equilibrium uptake deduced from these three samples, approximately 15 mass% of ZIF-8 was grown on the ZIF-L in the core−shell composites. This is in good agreement with the ZIF-8 mass fraction derived using nitrogen physisorption. Contrary to what has been suggested in the literature,[52] our results showed that the CO_2 equilibrium uptake of ZIF-L was far lower than that of ZIF-8. This inconsistency is

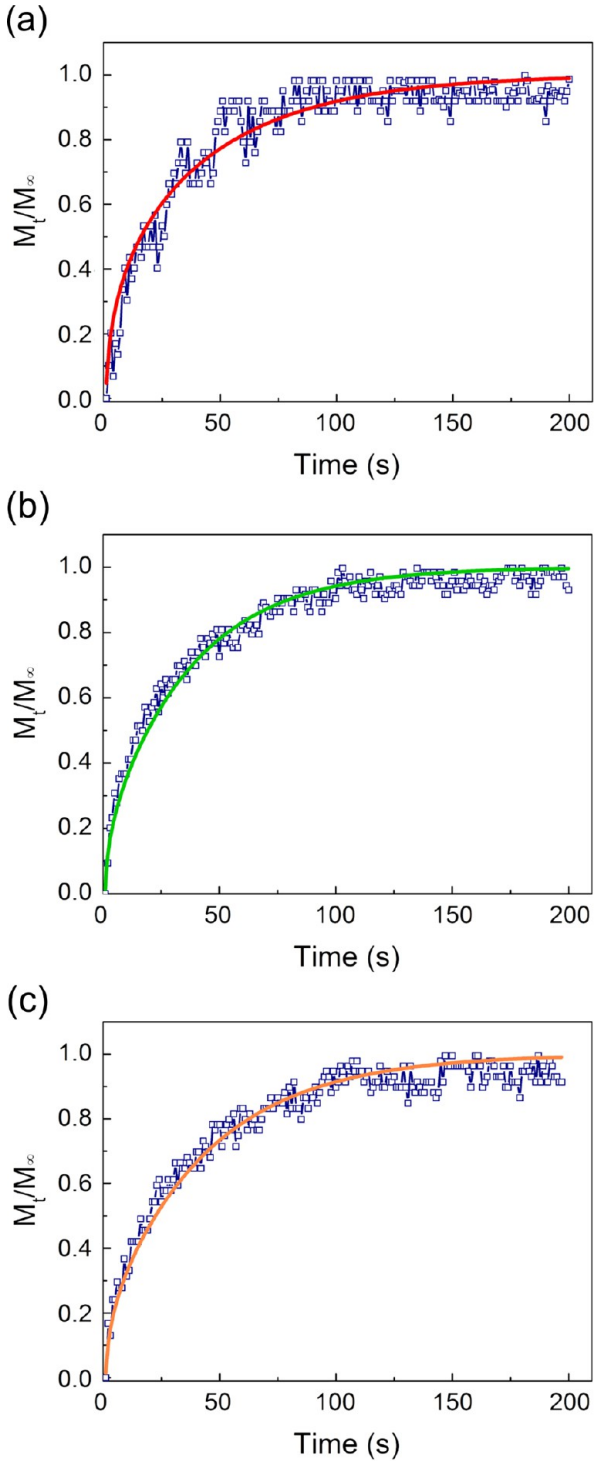

Figure 7. Dynamics involved in normalized CO_2 adsorption quantity: (a) ZIF-8, (b) ZIF-L, and (c) ZIF-L@ZIF-8 core−shell nanocomposites. The open squares represent experiment data and the curves are the best-fitting results from the transient adsorption models.

Table 1. CO_2 Uptake and Diffusivity at 5.6 Torr

property	ZIF-L	ZIF-L@ZIF-8	ZIF-8
CO_2 uptake (cm^3/g STP)	0.069	0.143	0.552
diffusivity (nm^2/s)	207	675	1217

DOI: 10.1021/acsami.5b04217
ACS Appl. Mater. Interfaces 2015, 7, 18353−18361

likely because adsorption tests in the previous report were performed under relatively high pressure conditions (>100 kPa), whereas the measurements in this study were obtained at 5.6 Torr. According to previous reports, the framework in ZIF materials can be highly flexible, such that the adsorption properties may differ considerably under different pressure conditions. Similarly, the diffusivity of ZIF-8 deduced in this study is lower than previously reported values,[63−65] which is likely due to the far lower pressures applied in our experiments. One interesting observation related to the diffusivity of these materials was that despite the fact that ZIF-L and the core−shell crystals both have significantly lower diffusivity than ZIF-8, the time scales required for all three materials to reach equilibrium were very similar. This is likely due to the fact that the characteristic length of the ZIF-L crystals and core−shell nanocomposites for CO_2 diffusion are far smaller than the ZIF-8 crystals. Reducing the size of ZIF-8 crystals is feasible; however, small crystals would likely create an undesirably large drop in pressure in practical adsorption applications. In cases of diffusion in layered materials, larger crystals with small characteristic lengths could potentially minimize the pressure drop while simultaneously maximizing adsorption kinetics. Thus, core−shell nanocomposites with layered ZIF-L as the core material could enable the rational engineering of high-performance ZIF-based adsorbents.

CONCLUSION

This study presents a new approach to engineering the crystal shape of zeolitic imidazolate frameworks (ZIFs) through the synthesis of core−shell nanocomposites. The near-spherical crystal morphology of ZIF-8 is transformed through the heterogeneous surface growth of a uniform thin layer on a nanoflake pseudopolymorph, ZIF-L. This resulted in ZIF-L@ZIF-8 core−shell nanocomposites with a nanosheet structure, as confirmed using a number of solid-state characterization techniques, including powder X-ray diffraction, scanning electron microscopy, thermogravimetric analysis, and nitrogen physisorption. We also evaluated the effects of zinc salts on the formation of the ZIF-L@ZIF-8 core−shell nanocomposites. We discovered that using $Zn(NO_3)_2$ or $Zn(OAc)_2$ as the zinc source for the heterogeneous surface growth of ZIF-8 yielded core−shell crystals, whereas $Zn(acac)_2$ and ZnCl had detrimental effects on the ZIF-L core crystals, which prevented the formation of the core−shell composites. CO_2 adsorption measurements were performed on ZIF-8, ZIF-L, and ZIF-L@ZIF-8 core−shell crystals in order to deduce CO_2 diffusivity and equilibrium adsorption uptake. We determined that the ZIF-L@ZIF-8 core−shell nanocomposites possessed the hybridized adsorption properties of its parent materials. These findings into the shaping of ZIF-8 into thin-layer crystals open up new possibilities for the creation of low-dimensional ZIF crystals. The synthesis of core−shell nanocomposites using pseudopolymorphic crystals could also enable the discovery of new ZIF-based hybrid materials.

ASSOCIATED CONTENT

Supporting Information

The Supporting Information is available free of charge on the ACS Publications website at DOI: 10.1021/acsami.5b04217.

Additional SEM images of the ZIF-L crystals and ZIF-L@ZIF-8 nanocomposites and the results of thermogravimetric analysis and FT-IR spectra of various crystals, as well as SEM images of ZIF crystals used for CO_2 adsorption (PDF)

AUTHOR INFORMATION

Corresponding Author

*E-mail: dunyen@ntu.edu.tw.

Notes

The authors declare no competing financial interest.

ACKNOWLEDGMENTS

This work was jointly supported by the Ministry of Science and Technology (MOST) of Taiwan (NSC 102-2218-E-002-015-MY2, MOST 104-2218-E-002-006, and MOST 104-2628-E-002-009-MY3) and National Taiwan University (NTU-CDP-104R7814).

REFERENCES

(1) Phan, A.; Doonan, C. J.; Uribe-Romo, F. J.; Knobler, C. B.; O'Keeffe, M.; Yaghi, O. M. Synthesis, Structure, and Carbon Dioxide Capture Properties of Zeolitic Imidazolate Frameworks. *Acc. Chem. Res.* **2010**, *43*, 58−67.

(2) Lewis, D. W.; Ruiz-Salvador, A. R.; Gomez, A.; Rodriguez-Albelo, L. M.; Coudert, F.-X.; Slater, B.; Cheetham, A. K.; Mellot-Draznieks, C. Zeolitic Imidazole Frameworks: Structural and Energetics Trends Compared with Their Zeolite Analogues. *CrystEngComm* **2009**, *11*, 2272−2276.

(3) Tian, Y.-Q.; Chen, Z.-X.; Weng, L.-H.; Guo, H.-B.; Gao, S.; Zhao, D. Y. Two Polymorphs of Cobalt(Ii) Imidazolate Polymers Synthesized Solvothermally by Using One Organic Template N,N-Dimethylacetamide. *Inorg. Chem.* **2004**, *43*, 4631−4635.

(4) Pimentel, B. R.; Parulkar, A.; Zhou, E.-k.; Brunelli, N. A.; Lively, R. P. Zeolitic Imidazolate Frameworks: Next-Generation Materials for Energy-Efficient Gas Separations. *ChemSusChem* **2014**, *7*, 3202−3240.

(5) Liu, Y.; Zeng, G.; Pan, Y.; Lai, Z. Synthesis of Highly C-Oriented ZIF-69 Membranes by Secondary Growth and Their Gas Permeation Properties. *J. Membr. Sci.* **2011**, *379*, 46−51.

(6) Li, Y.-S.; Liang, F.-Y.; Bux, H.; Feldhoff, A.; Yang, W.-S.; Caro, J. Molecular Sieve Membrane: Supported Metal−Organic Framework with High Hydrogen Selectivity. *Angew. Chem., Int. Ed.* **2010**, *49*, 548−551.

(7) Banerjee, R.; Phan, A.; Wang, B.; Knobler, C.; Furukawa, H.; O'Keeffe, M.; Yaghi, O. M. High-Throughput Synthesis of Zeolitic Imidazolate Frameworks and Application to CO_2 Capture. *Science* **2008**, *319*, 939−943.

(8) Li, J.-R.; Kuppler, R. J.; Zhou, H.-C. Selective Gas Adsorption and Separation in Metal-Organic Frameworks. *Chem. Soc. Rev.* **2009**, *38*, 1477−1504.

(9) Seo, J. S.; Whang, D.; Lee, H.; Jun, S. I.; Oh, J.; Jeon, Y. J.; Kim, K. A Homochiral Metal-Organic Porous Material for Enantioselective Separation and Catalysis. *Nature* **2000**, *404*, 982−986.

(10) Shimizu, G. K. H.; Vaidhyanathan, R.; Taylor, J. M. Phosphonate and Sulfonate Metal Organic Frameworks. *Chem. Soc. Rev.* **2009**, *38*, 1430−1449.

(11) Lee, J.; Farha, O. K.; Roberts, J.; Scheidt, K. A.; Nguyen, S. T.; Hupp, J. T. Metal-Organic Framework Materials as Catalysts. *Chem. Soc. Rev.* **2009**, *38*, 1450−1459.

(12) Ma, L.; Abney, C.; Lin, W. Enantioselective Catalysis with Homochiral Metal-Organic Frameworks. *Chem. Soc. Rev.* **2009**, *38*, 1248−1256.

(13) Morris, R. E.; Wheatley, P. S. Gas Storage in Nanoporous Materials. *Angew. Chem., Int. Ed.* **2008**, *47*, 4966−4981.

(14) Rosi, N. L.; Eckert, J.; Eddaoudi, M.; Vodak, D. T.; Kim, J.; O'Keeffe, M.; Yaghi, O. M. Hydrogen Storage in Microporous Metal-Organic Frameworks. *Science* **2003**, *300*, 1127−1129.

(15) Murray, L. J.; Dinca, M.; Long, J. R. Hydrogen Storage in Metal-Organic Frameworks. *Chem. Soc. Rev.* **2009**, *38*, 1294−1314.

DOI: 10.1021/acsami.5b04217
ACS Appl. Mater. Interfaces 2015, 7, 18353−18361

(16) Lai, Z. P.; Bonilla, G.; Diaz, I.; Nery, J. G.; Sujaoti, K.; Amat, M. A.; Kokkoli, E.; Terasaki, O.; Thompson, R. W.; Tsapatsis, M.; Vlachos, D. G. Microstructural Optimization of a Zeolite Membrane for Organic Vapor Separation. *Science* **2003**, *300*, 456−460.
(17) Freyhardt, C. C.; Tsapatsis, M.; Lobo, R. F.; Balkus, K. J.; Davis, M. E. A High-Silica Zeolite with a 14-Tetrahedral-Atom Pore Opening. *Nature* **1996**, *381*, 295−298.
(18) Davis, T. M.; Drews, T. O.; Ramanan, H.; He, C.; Dong, J. S.; Schnablegger, H.; Katsoulakis, M. A.; Kokkoli, E.; McCormick, A. V.; Penn, R. L.; Tsapatsis, M. Mechanistic Principles of Nanoparticle Evolution to Zeolite Crystals. *Nat. Mater.* **2006**, *5*, 400−408.
(19) Davis, M. E.; Lobo, R. F. Zeolite and Molecular Sieve Synthesis. *Chem. Mater.* **1992**, *4*, 756−768.
(20) Snyder, M. A.; Tsapatsis, M. Hierarchical Nanomanufacturing: From Shaped Zeolite Nanoparticles to High-Performance Separation Membranes. *Angew. Chem., Int. Ed.* **2007**, *46*, 7560−7573.
(21) Brown, A. J.; Brunelli, N. A.; Eum, K.; Rashidi, F.; Johnson, J. R.; Koros, W. J.; Jones, C. W.; Nair, S. Interfacial Microfluidic Processing of Metal-Organic Framework Hollow Fiber Membranes. *Science* **2014**, *345*, 72−75.
(22) Shah, M.; McCarthy, M. C.; Sachdeva, S.; Lee, A. K.; Jeong, H.-K. Current Status of Metal−Organic Framework Membranes for Gas Separations: Promises and Challenges. *Ind. Eng. Chem. Res.* **2012**, *51*, 2179−2199.
(23) Pan, Y.; Li, T.; Lestari, G.; Lai, Z. Effective Separation of Propylene/Propane Binary Mixtures by ZIF-8 Membranes. *J. Membr. Sci.* **2012**, *390*−*391*, 93−98.
(24) Li, Y.; Liang, F.; Bux, H.; Yang, W.; Caro, J. Zeolitic Imidazolate Framework ZIF-7 Based Molecular Sieve Membrane for Hydrogen Separation. *J. Membr. Sci.* **2010**, *354*, 48−54.
(25) Choi, M.; Cho, H. S.; Srivastava, R.; Venkatesan, C.; Choi, D.-H.; Ryoo, R. Amphiphilic Organosilane-Directed Synthesis of Crystalline Zeolite with Tunable Mesoporosity. *Nat. Mater.* **2006**, *5*, 718−723.
(26) Choi, M.; Na, K.; Kim, J.; Sakamoto, Y.; Terasaki, O.; Ryoo, R. Stable Single-Unit-Cell Nanosheets of Zeolite Mfi as Active and Long-Lived Catalysts. *Nature* **2009**, *461*, 246−249.
(27) Lee, P.-S.; Zhang, X.; Stoeger, J. A.; Malek, A.; Fan, W.; Kumar, S.; Yoo, W. C.; Al Hashimi, S.; Penn, R. L.; Stein, A.; Tsapatsis, M. Sub-40 Nm Zeolite Suspensions Via Disassembly of Three-Dimensionally Ordered Mesoporous-Imprinted Silicalite-1. *J. Am. Chem. Soc.* **2011**, *133*, 493−502.
(28) Zhang, X.; Liu, D.; Xu, D.; Asahina, S.; Cychosz, K. A.; Agrawal, K. V.; Al Wahedi, Y.; Bhan, A.; Al Hashimi, S.; Terasaki, O.; Thommes, M.; Tsapatsis, M. Synthesis of Self-Pillared Zeolite Nanosheets by Repetitive Branching. *Science* **2012**, *336*, 1684−1687.
(29) Chaikittisilp, W.; Suzuki, Y.; Mukti, R. R.; Suzuki, T.; Sugita, K.; Itabashi, K.; Shimojima, A.; Okubo, T. Formation of Hierarchically Organized Zeolites by Sequential Intergrowth. *Angew. Chem., Int. Ed.* **2013**, *52*, 3355−3359.
(30) Perez-Ramirez, J.; Christensen, C. H.; Egeblad, K.; Christensen, C. H.; Groen, J. C. Hierarchical Zeolites: Enhanced Utilisation of Microporous Crystals in Catalysis by Advances in Materials Design. *Chem. Soc. Rev.* **2008**, *37*, 2530−2542.
(31) Serrano, D. P.; Escola, J. M.; Pizarro, P. Synthesis Strategies in the Search for Hierarchical Zeolites. *Chem. Soc. Rev.* **2013**, *42*, 4004−4035.
(32) Inayat, A.; Knoke, I.; Spiecker, E.; Schwieger, W. Assemblies of Mesoporous Fau-Type Zeolite Nanosheets. *Angew. Chem., Int. Ed.* **2012**, *51*, 1962−1965.
(33) Corma, A.; Fornes, V.; Pergher, S. B.; Maesen, T. L. M.; Buglass, J. G. Delaminated Zeolite Precursors as Selective Acidic Catalysts. *Nature* **1998**, *396*, 353−356.
(34) Gomez, A. G.; Silveira, G. d.; Doan, H.; Cheng, C.-H. A Facile Method to Tune Zeolite L Crystals with Low Aspect Ratio. *Chem. Commun.* **2011**, *47*, 5876−5878.
(35) Kim, W.-g.; Nair, S. Membranes from Nanoporous 1d and 2d Materials: A Review of Opportunities, Developments, and Challenges. *Chem. Eng. Sci.* **2013**, *104*, 908−924.
(36) Kim, W.-g.; Zhang, X.; Lee, J. S.; Tsapatsis, M.; Nair, S. Epitaxially Grown Layered MFI−Bulk MFI Hybrid Zeolitic Materials. *ACS Nano* **2012**, *6*, 9978−9988.
(37) Kubů, M.; Roth, W. J.; Greer, H. F.; Zhou, W.; Morris, R. E.; Přech, J.; Čejka, J. A New Family of Two-Dimensional Zeolites Prepared from the Intermediate Layered Precursor Ipc-3p Obtained During the Synthesis of Tun Zeolite. *Chem. - Eur. J.* **2013**, *19*, 13937−13945.
(38) Leonowicz, M. E.; Lawton, J. A.; Lawton, S. L.; Rubin, M. K. MCM-22: A Molecular Sieve with Two Independent Multidimensional Channel Systems. *Science* **1994**, *264*, 1910−1913.
(39) Bouizi, Y.; Rouleau, L.; Valtchev, V. P. Factors Controlling the Formation of Core−Shell Zeolite−Zeolite Composites. *Chem. Mater.* **2006**, *18*, 4959−4966.
(40) Goossens, A. M.; Wouters, B. H.; Buschmann, V.; Martens, J. A. Oriented Fau Zeolite Films on Micrometer-Sized Emt Crystals. *Adv. Mater.* **1999**, *11*, 561−564.
(41) Wang, Z.; Wan, W.; Sun, J.; Carrillo-Cabrera, W.; Gruner, D.; Yin, X.; Qiu, S.; Zhu, G.; Zou, X. Epitaxial Growth of Core-Shell Zeolite X-a Composites. *CrystEngComm* **2012**, *14*, 2204−2212.
(42) Yonkeu, A. L.; Miehe, G.; Fuess, H.; Goossens, A. M.; Martens, J. A. A New Overgrowth of Mazzite on Faujasite Zeolite Crystal Investigated by X-Ray Diffraction and Electron Microscopy. *Microporous Mesoporous Mater.* **2006**, *96*, 396−404.
(43) Shi, Q.; Song, Z. W.; Kang, X. Z.; Dong, J. X.; Zhang, Y. Controlled Synthesis of Hierarchical Zeolitic Imidazolate Framework-Gis (ZIF-Gis) Architectures. *CrystEngComm* **2012**, *14*, 8280−8285.
(44) Wee, L. H.; Lescouet, T.; Ethiraj, J.; Bonino, F.; Vidruk, R.; Garrier, E.; Packet, D.; Bordiga, S.; Farrusseng, D.; Herskowitz, M.; Martens, J. A. Hierarchical Zeolitic Imidazolate Framework-8 Catalyst for Monoglyceride Synthesis. *ChemCatChem* **2013**, *5*, 3562−3566.
(45) Wu, Y. N.; Zhou, M. M.; Zhang, B. R.; Wu, B. Z.; Li, J.; Qiao, J. L.; Guan, X. H.; Li, F. T. Amino Acid Assisted Templating Synthesis of Hierarchical Zeolitic Imidazolate Framework-8 for Efficient Arsenate Removal. *Nanoscale* **2014**, *6*, 1105−1112.
(46) Zhang, T.; Zhang, X.; Yan, X.; Lin, L.; Liu, H.; Qiu, J.; Yeung, K. L. Core−Shell Pd/ZSM-5@ZIF-8 Membrane Micro-Reactors with Size Selectivity Properties for Alkene Hydrogenation. *Catal. Today* **2014**, *236*, 41−48.
(47) Lee, H. J.; Cho, W.; Oh, M. Advanced Fabrication of Metal-Organic Frameworks: Template-Directed Formation of Polystyrene@ ZIF-8 Core-Shell and Hollow ZIF-8 Microspheres. *Chem. Commun.* **2012**, *48*, 221−223.
(48) Tang, J.; Salunkhe, R. R.; Liu, J.; Torad, N. L.; Imura, M.; Furukawa, S.; Yamauchi, Y. Thermal Conversion of Core−Shell Metal−Organic Frameworks: A New Method for Selectively Functionalized Nanoporous Hybrid Carbon. *J. Am. Chem. Soc.* **2015**, *137*, 1572−1580.
(49) Li, Z.; Zeng, H. C. Surface and Bulk Integrations of Single-Layered Au or Ag Nanoparticles onto Designated Crystal Planes {110} or {100} of ZIF-8. *Chem. Mater.* **2013**, *25*, 1761−1768.
(50) Pan, Y.; Heryadi, D.; Zhou, F.; Zhao, L.; Lestari, G.; Su, H.; Lai, Z. Tuning the Crystal Morphology and Size of Zeolitic Imidazolate Framework-8 in Aqueous Solution by Surfactants. *CrystEngComm* **2011**, *13*, 6937−6940.
(51) Schejn, A.; Balan, L.; Falk, V.; Aranda, L.; Medjahdi, G.; Schneider, R. Controlling ZIF-8 Nano- and Microcrystal Formation and Reactivity through Zinc Salt Variations. *CrystEngComm* **2014**, *16*, 4493−4500.
(52) Chen, R.; Yao, J.; Gu, Q.; Smeets, S.; Baerlocher, C.; Gu, H.; Zhu, D.; Morris, W.; Yaghi, O. M.; Wang, H. A Two-Dimensional Zeolitic Imidazolate Framework with a Cushion-Shaped Cavity for Co2 Adsorption. *Chem. Commun.* **2013**, *49*, 9500−9502.
(53) Low, Z.-X.; Yao, J.; Liu, Q.; He, M.; Wang, Z.; Suresh, A. K.; Bellare, J.; Wang, H. Crystal Transformation in Zeolitic-Imidazolate Framework. *Cryst. Growth Des.* **2014**, *14*, 6589−6598.
(54) Low, Z.-X.; Razmjou, A.; Wang, K.; Gray, S.; Duke, M.; Wang, H. Effect of Addition of Two-Dimensional ZIF-L Nanoflakes on the

DOI: 10.1021/acsami.5b04217
ACS Appl. Mater. Interfaces 2015, 7, 18353−18361

Properties of Polyethersulfone Ultrafiltration Membrane. *J. Membr. Sci.* **2014**, *460*, 9−17.
(55) Venna, S.; Zhu, M.; Li, S.; Carreon, M. Knudsen Diffusion through ZIF-8 Membranes Synthesized by Secondary Seeded Growth. *J. Porous Mater.* **2014**, *21*, 235−240.
(56) Pan, Y.; Liu, Y.; Zeng, G.; Zhao, L.; Lai, Z. Rapid Synthesis of Zeolitic Imidazolate Framework-8 (ZIF-8) Nanocrystals in an Aqueous System. *Chem. Commun.* **2011**, *47*, 2071−2073.
(57) Jian, M.; Liu, B.; Liu, R.; Qu, J.; Wang, H.; Zhang, X. Water-Based Synthesis of Zeolitic Imidazolate Framework-8 with High Morphology Level at Room Temperature. *RSC Adv.* **2015**, *5*, 48433−48441.
(58) Bustamante, E. L.; Fernandez, J. L.; Zamaro, J. M. Influence of the Solvent in the Synthesis of Zeolitic Imidazolate Framework-8 (ZIF-8) Nanocrystals at Room Temperature. *J. Colloid Interface Sci.* **2014**, *424*, 37−43.
(59) Tanaka, S.; Kida, K.; Okita, M.; Ito, Y.; Miyake, Y. Size-Controlled Synthesis of Zeolitic Imidazolate Framework-8 (ZIF-8) Crystals in an Aqueous System at Room Temperature. *Chem. Lett.* **2012**, *41*, 1337−1339.
(60) Kida, K.; Okita, M.; Fujita, K.; Tanaka, S.; Miyake, Y. Formation of High Crystalline Zif-8 in an Aqueous Solution. *CrystEngComm* **2013**, *15*, 1794−1801.
(61) Hines, A. L.; Maddox, R. N. *Mass Transfer: Fundamentals and Applications*; Prentice-Hall: Englewood Cliffs, NJ, 1985.
(62) Thompson, J. A.; Brunelli, N. A.; Lively, R. P.; Johnson, J. R.; Jones, C. W.; Nair, S. Tunable CO_2 Adsorbents by Mixed-Linker Synthesis and Postsynthetic Modification of Zeolitic Imidazolate Frameworks. *J. Phys. Chem. C* **2013**, *117*, 8198−8207.
(63) Bux, H.; Chmelik, C.; van Baten, J. M.; Krishna, R.; Caro, J. Novel Mof-Membrane for Molecular Sieving Predicted by Ir-Diffusion Studies and Molecular Modeling. *Adv. Mater.* **2010**, *22*, 4741−4743.
(64) Haldoupis, E.; Watanabe, T.; Nair, S.; Sholl, D. S. Quantifying Large Effects of Framework Flexibility on Diffusion in Mofs: Ch4 and Co2 in ZIF-8. *ChemPhysChem* **2012**, *13*, 3449−3452.
(65) Zheng, B.; Sant, M.; Demontis, P.; Suffritti, G. B. Force Field for Molecular Dynamics Computations in Flexible ZIF-8 Framework. *J. Phys. Chem. C* **2012**, *116*, 933−938.

DOI: 10.1021/acsami.5b04217
ACS Appl. Mater. Interfaces 2015, 7, 18353−18361